Estimation of Maximum Inclusion Size and Fatigue Limit in HSLA-100 Steel

A. Abyazi [*1] , A. R. Ebrahimi [2]

[1] *Azarbaijan Shahid Madani University*
[2] *Department of Materials and Metallurgical engineering, Amirkabir University of Technology, Tehran, 158754413, Iran*

Abstract

The objective of the current study is to determine the fatigue limit of a clean and high performance material named as HSLA-100 steel, and to compare the obtained fatigue limit with that of theoretically predicted fatigue limit by statistics of extreme value (SEV) method. Also the size of inclusions located at the site of fatigue crack nucleation on the fracture surface of the fatigue test specimens was compared with the results of extreme value distribution of the inclusions as well as with that of analysis of inclusions found on polished specimen. The fatigue cracks were initiated from spherical inclusions in all fatigue test specimens. Analyzing the fatigue results showed that the SEV method can conservatively predict the planar fatigue limit of HSLA-100 steel. Also the largest inclusion size predicted by (SEV) method was larger than that of observed at fatigue crack initiation site as well as metallographic studies of polished specimens.

***Keywords*:** Statics of Extreme Values (SEV), Fatigue limit, HSLA-100 steel, Non-metallic inclusion size.

1. Introduction

The application of new secondary refining techniques[1,2] and also inclusion reduction techniques [3,4] in steel making processes have greatly reduced the amount and the size of non-metallic inclusions in steels. These ever-growing improvements in the newly developed high performance steels have already changed their inclusions characteristics, i.e., these clean steels consist of few large inclusions and plenty of small ones. This progress in clean steels has created in turn two principal problems. It reduces the usefulness of conventional inclusion inspection methods [5-7], so the assessment of inclusions essentially depends on statistical probabilistic analysis. It is well understood that the fatigue strength and endurance of steels are strongly affected by the largest inclusions contained in component. Because of the less probability to be present of large inclusions in fatigue test specimens of clean steels, their fatigue properties are highly scattered and so, as the second problem, demand unrealistically large numbers of tests.

Because of these two principal problems, attentions are being increasingly focused on the estimation of the largest inclusion that can be found in a steel component. Consequently, new inclusion rating methods are developed to detect and to estimate the largest size of non-metallic inclusions in any volume of metals [8-10]. Of them, the statistics of extremes value (SEV) method is one of the most reliable and quantitative one that can predict the characteristic dimension of the maximum inclusion size contained in component as well as its lower fatigue limit. The essential procedure of SEV method is reported by

** Corresponding author*
Email: ac.abyazi@azaruniv.ac.ir
Tell: +98 413 1452554
Address: Azarbaijan Shahid Madani University
1. Assistant Professor
2. Associate Professor

Y. Murakami [11] and is standardized in the ASTM E2283 standard [12].

HSLA-100 steel as a high performance clean steel is used in large-scale welded constructions owing to its higher strength, improved toughness and excellent weldability. This steel is used in the construction of naval warships and submarines and also for engineering bodies such as offshore drilling platforms, vessels, bridges, etc.[13, 14]. In the present study rotating bending fatigue test was performed by utilizing a clean HSLA-100 steel. Also the largest possible inclusion size and the theoretically lower bound fatigue limit were calculated and predicted using the SEV method. Finally for the validation of SEV method for its application to HSLA-100 steel, the size of the inclusions identified at the fatigue crack initiation site by the use of fractographic studies as well as the obtained fatigue limit from fatigue test results were compared with that of SEV results.

2. Materials and Methods

This study was carried out on an as received hot-rolled HSLA-100 steel plate and its chemical composition is given in Table 1. To determine the inclusions characteristics (i.e. morphology, type, count, size, area fraction and aspect ratio), 600 optical microscopic images were examined and analyzed by Clemex image analysis software. In order to estimate the largest possible inclusion size of the current material, the inclusion rating method based on statistics of extreme value (SEV) was used [11,15]. Nikon Eclipse L150 microscope with digital imaging system was set at 100× magnification. A standard area, S_0, was 1.1 mm^2 which corresponds to an area of one micrograph. The affected area of inclusion ($\sqrt{area}_{max}$), i.e., the size of the largest inclusion, has been measured in each standard area. Totally 40 unit areas were examined on each polished plane according to the suggestions in the Murakami-Endo method [9]. The fatigue specimens were prepared according to DIN50113. Fatigue tests with hourglass shaped specimens with a gauge diameter of 5 mm were conducted on a rotary bending fatigue test machine (model: Roell Amsler UBM 200) at 3000 rpm. All of the tests were done with stress ratio of R=−1 in laboratory at ambient temperature. In case a fatigue test specimen reached the run out limit (10^7 cycles), then that specimen was retested at a stress level about 50-100 MPa higher than that of run out stress level. This process was done in order to cause the failure of run out specimens so that the largest inclusion which was responsible for fatigue failure, could be found. The fractographic studies of broken specimens were carried out using a MV 2300 Cam Scan field-emission scanning electron microscopy (SEM). The average hardness of HSLA-100 steel is 253.2±5.5 *H*v.

Table 1. Chemical Composition (In Weight Percent) of the HSLA-100 steel.

C	Mn	Si	P	S	Cu	Cr	Mo	Ni	Nb	Ti	V
0.04	0.78	0.25	0.008	0.006	1.72	0.62	0.64	3.55	0.033	0.009	0.015

3. Results and discussion

3. 1. Non-metallic inclusions

Based mainly on their morphological observations, three kinds of non-metallic inclusions were identified in the current HSLA-100 steel by analyzing 600 microscopic images. (a) Spherical-shaped inclusions containing Al, O, Ca, Mn and S; (b) elongated manganese sulfide inclusions and (c) complex type ones at which elongated inclusions crossed the spherical types. A typical example of these inclusions is illustrated in Fig. 1. Characteristics (type, size, area fraction and aspect ratio) of these inclusions are introduced in Table 2. To complete the data of the Table given below, the characteristics of about 8450 non-metallic inclusions were extracted by analyzing 600 microscopic images. According to the data introduced in the Table almost 99.7% of inclusions in HSLA-100 steel were morphologically spherical and also very small (typically smaller than 5 μm). As shown in Table 2, fewer counts of elongated inclusions also were obtained in the current material. These MnS inclusions are severely elongated with apparent lengths of between 20-170 μm. However these inclusions contain less than 1 μm width and therefore fall into the category of thin [1] inclusions. As shown in Fig. 1 (a), the spherical inclusions composed of two parts: the inner part completely dark and the surrounding area seems brighter (almost gray). This kind of spherical inclusions which are recognized as "bull's-eye", are formed by addition of Ca for modifying the inclusion shape [16]. As reported in detail previously [14], results of dispersive X-ray (EDAX) analysis has already shown that the central region of spherical inclusions of the current HSLA-100 steel was an aluminate phase and the peripheral region composed of a manganese sulfide

1. As stated in ASTM E45 standard, the term "thin inclusion" is used when the width of an elongated inclusion is less than 10μm for the most part of its length (more than half of length inclusion).

phase containing calcium. Other researchers have also made similar findings in two other calcium-treated steel [17]. These duplex inclusions (Aluminate and (Ca, Mn) S) are modified along with Ca-treatment operation during inclusion refining of the current material. Researchers have shown that Ca-treatment plays two essential roles in steels: converting the solid aluminum oxide inclusions to lower melting point calcium aluminates as well as modifying the inclusions into spherical shape from stringer type morphology [18]. However, as shown in Figs. 1(b) and 1(c) some elongated-type inclusions may also sporadically obtain in calcium treated steels. The presence of these stringer-type inclusions in calcium treated steels is a major unsolved problem in industrial practices indicates that calcium addition may not completely encapsulate all the MnS inclusions [18, 19].

Table 2. The characteristics* of inclusions in HSLA-100 steel.

Morphology	Type	Count	Average Size (μm)	Average area fraction	Average aspect ratio
Spherical	Aluminate and (Ca, Mn)S)	8442	4.7±1.2	0.029±0.001	1.40±0.06
Elongated	MnS	12	43.3±31.2	0.002±0.002	75.5±55.1
Combined	(Aluminate and (Ca, Mn)S) + MnS	9	34.1±20.6	0.013±0.008	7.9±4.6
* characteristics are extracted by analyzing 600 microscopic images					

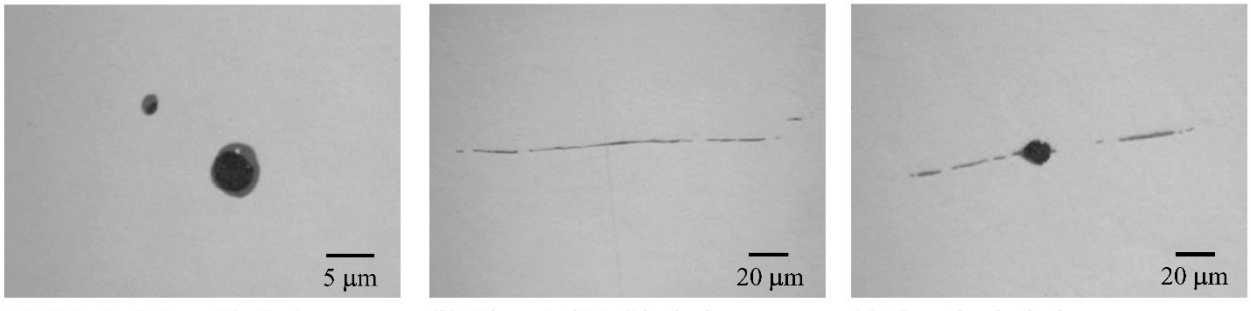

(a): Spherical-shaped inclusions (b): Elongated MnS inclusions (c): Complex inclusions

Fig. 1. Inclusions morphology of HSLA-100 steel.

3. 2. Statics of Extreme Values (SEV)

Fig. 2 shows a bi-linear form of largest extreme-value distribution (LEVD) [20,21] taking into account the presence of two inclusion types with distinct slopes of the largest inclusions in HSLA-100 steel. Inclusion sampling had been carried out with control areas, S_0 = 1.1 mm^2 and the sizes of inclusions had been measured in terms of the square root of area ($\sqrt{area}_{max}$). The vertical axis of the graph shows the cumulative distribution frequency, reduced variate and return period. The horizontal axis shows the $\sqrt{area}_{max}$ values. Research findings obtained by some researchers has revealed a large difference in the logarithmic distribution curves for oxide and sulfide inclusions [22, 23]. According to Fig. 2 despite a little difference, the slope of curves related to the oxide and sulfide inclusions in the current HSLA-100 steel is not significantly different. One probable reason may be related to the very thin thickness of MnS inclusions in the current clean steel compared to that of others. Taking into account the shape and dimensions of the fatigue sample used in this study (R = 12.5 mm and d=5 mm) the regression linear equation is described as $\sqrt{area}_{max}$=5.738 y + 11.34 ≈ 39 μm. So The SEV method predicts the largest possible size of non-metallic inclusion in the current HSLA-100 steel as $\sqrt{area}_{max}$=39 μm.

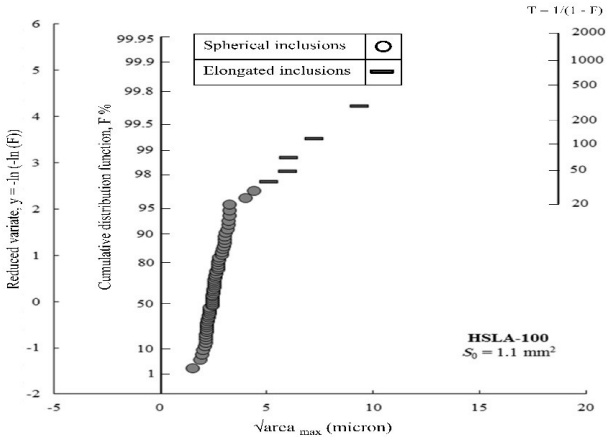

Fig. 2. Statics of Extreme Values (SEV) distribution of inclusions in HSLA-100 steel.

3. 3. Prediction of the lower band of the fatigue limit

In addition to the possibility of predicting the largest non-metallic inclusions, the extreme value distribution analysis is also used to predict the theoretical lower fatigue limit of the steel. The Murakami–Endo Model predicts that when the location of the fracture origin is a non-metallic inclusion then the fatigue limit of the material can be determined by the Vickers hardness of the microstructure surrounding the non-metallic inclusion and the square root of the projected √area of the defect normal to the stress. Detailed description of the procedure is provided in reference document [15]. Applying this model and expecting fatigue crack initiation from interior (subsurface) inclusion the theoretical lower fatigue limit of HSLA-100 was calculated to be 315.6 MPa, with a standard deviation of ±4.2 MPa.

3. 4. Fatigue test results

The results of the fatigue tests are shown in Fig. 3. The rotating bending fatigue tests were performed at room temperature and the run out limit was set at 10^7 cycles (as indicated in the figure). If a test bar reached the run out limit (10^7 cycles) then the fatigue test was stopped and classified as a run out. All of the run out bars were retested at stress level that was 50-100 MPa higher than the run out stress level. This was done to have the fatigue failure taken place so that the largest inclusion causing failure could be studied. The lower fatigue limit predicted by statistics of extremes value (SEV) rating method is also shown beside the fatigue test results in the figure. As shown in the figure all the fatigue tests failed above the theoretical lower bound limit predicted by SEV analysis. Therefore the prediction of the lower bound fatigue limit according to the Murakami–Endo model provided a conservative estimate for HSLA-100 steel. According to Fig. 3, theoretical lower fatigue limit (~ 315.6 MPa) of HSLA-100 is significantly lower than fatigue limit (~525 MPa) obtained by fatigue tests.

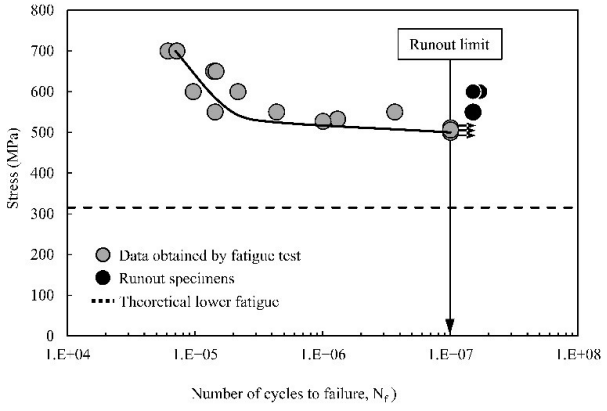

Fig. 3. S-N curve of HSLA-100 steel.

3. 5. Fractography

Fatigue crack initiation site of all three retested runout specimens was investigated employing electron microscopy. In all retested run-outs, defects smaller than 15 microns were obtained slightly below the surface. An example of these defects is given in the Fig. 4. It is shown that an approximately globular defect with root area of 13.5 μm is located almost 20 microns inner site from the surface. The effective size (root area) of two other defects was 9 and 10.5 μm. Interestingly, it is observed that the size of inclusions responsible for fatigue crack initiation are conservatively smaller than that of predicted largest inclusion size (39 μm) with SEV method in fatigue specimens of the current material. Juvonen and Roiko have found similar results with studying on calcium-treated steels [24, 25]. The EDX analysis results taken from this area are given in Fig. 5. According to this figure, a concentration of aluminum, oxygen, manganese, sulfur and calcium is observed in EDX results. Correspondingly these defects are non-metallic inclusion composed of an aluminate phase at the center and a manganese sulfide phase containing calcium in its surrounding areas. As indicated earlier, these are typical duplex non-metallic inclusions (Aluminate and (Ca, Mn) S) which are modified during calcium-treatment process of HSLA-100 steels. The interesting consequence is that the spherical inclusions were the origin for fatigue crack initiation and no elongated manganese sulfide inclusion was observed in this site. Similar results (not to grow the fatigue crack from elongated inclusions in calcium-treated steels) have already observed by other researchers [24].

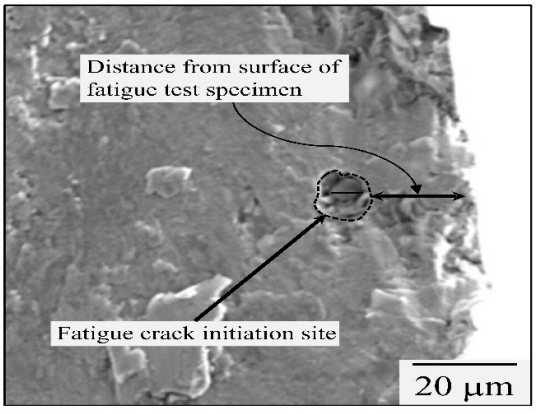

Fig. 4. Fatigue crack initiation site of HSLA-100 steel.

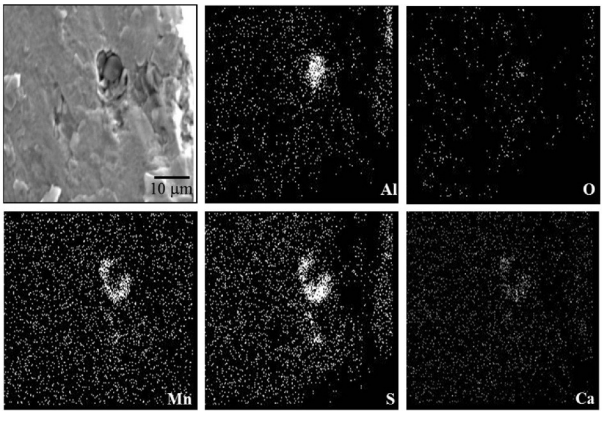

Fig. 5. EDX analysis of fatigue crack initiation area of fatigue specimen.

4. Conclusion

- The prediction of the lower bound fatigue limit according to the Murakami–Endo model provided a conservative estimate for the lower bound fatigue limit. All the fatigue tests failed above the predicted theoretically lower bound limit.
- Applying the statistics of extremes (SEV) to inclusions on polished specimen to predict the inclusion causing fatigue failure provided accurate and also very conservative results for the average inclusion size. The extreme value prediction for inclusions ($\sqrt{area}_{max}$=39 μm) was much larger than what was discovered on fatigue crack initiation site (smaller than 15 μm).
- Duplex (Aluminate and (Ca, Mn)S) non-metallic inclusions were observed at planar fatigue crack initiation site of the current HSLA-100 steel.

Nomenclature

$\sqrt{area}_{max}$ = extreme value of the inclusion size, mm;
d =diameter of the central part of fatigue test specimen, mm;
F = the cumulative distribution function;
HSLA = high strength low alloy;
HV = Vickers hardness;
N_f = number of cycles to fracture;
R = stress ratio;
S_0 = standard inspection area (or control area), mm^2;
SEV = statistics of extreme value;
T = return period;
y = reduced variate.

References

[1] D. Sichen: Steel Res. Int., 83(2012), 825.
[2] S. Taniguchi, J. K. Brimacombe: ISIJ Int., 34(1994), 722.
[3] V. Gollapalli, M.V. Rao, P.S. Karamched, C.R. Borra, G.G. Roy, P. Srirangam: Ironmaking & Steelmaking, 46(2019), 663.
[4] M. Imagumbai, T. Takeda: ISIJ Int., 34(1994), 574.
[5] ASTM E45: Standard Test Methods for Determining the Inclusion Content of Steel, (2007).
[6] J. Ogilvy: Ultrasonics: 31(1993), 219.
[7] Kato, S. Takemoto, K. Sato, Y. Nuri: Sanyo Tech. Rep., 7(2000), 35.
[8] Y. Murakami, S. Kodama, S. Konuma: Int. J. Fatigue., 11(1989), 291.
[9] Y. Murakami, M. Endo: Int. J. Fatigue., 16(1994), 163.
[10] G. Shi, H. Atkinson, C. Sellars, C. Anderson: Acta. Mater., 47(1999), 1455.
[11] Y. Murakami, T. Toriyama, E. CoudertL: J. Test. Eva., 22(1994), 318.
[12] ASTM E2283, Standard Practice for Extreme Value Analysis of Nonmetallic Inclusions in Steel and Other Microstructural Features, (2019).
[13] E. J. Czyryca, R.E. Link, R.J. Wong, D. A. Aylor, T. W. Montem, J. P. Gudas, Naval Eng. J., 102(1990), 63.
[14] A. Abyazi, A. Ebrahimi: Mater. Sci. Techn., 32(2016), 976.
[15] Y. Murakami: Metal Fatigue, effects of small defects and nonmetallic inclusions, Academic Press, (2019), 321.
[16] A. D. Wilson, Inclusions and their influence on material behavior, ASM International, Chicago, (1989).
[17] H. Du: The evaluation of non-metallic inclusions in calcium-treated steel by using electrolytic extraction, thesis,Stockholm, Sweden (2016).
[18] A. Costa e Silva: J. Mater. Res. Technol., 3(2018), 283.
[19] S. Putatunda, A. Christ, E. Cabadas, M. Shapona, K. Tatteff, M. Rao, SAE transactions, (1994), 153.
[20] S. Beretta, Y. Murakami: Metal. Mater. Trans. B., 32 (2001), 517.
[21] Y. Murakami, H. Matsunaga, A. Abyazi, Y. Fukushima, Fatig. Fract. Eng. Mater. Struct., 36(2013), 836.

[22] C.C. Hsu, H. H. Chung, Adv. Materi. Res., Trans. Tech. Publ., 939 (2014), 11.
[23] Y. Kanbe, A. Karasev, H. Todoroki, P. G. Jönsson: Steel Res. Int., 82(2011), 322.
[24] P. Juvonen, Effects of non-metallic inclusions on fatigue properties of calcium treated steels, thesis, Helsinki University of Technology, (2004).
[25] A. Roiko, H. Hänninen, H. Vuorikari, Int. J. Fat., 41(2012), 158.